



## GNSS Vertical Coordinate Time Series Analysis Using Single-Channel Independent Component Analysis Method

WEI PENG,<sup>1</sup> WUJIAO DAI,<sup>1</sup> ROCK SANTERRE,<sup>2</sup> CHANGSHENG CAI,<sup>1</sup> and CUILIN KUANG<sup>1</sup>

**Abstract**—Daily vertical coordinate time series of Global Navigation Satellite System (GNSS) stations usually contains tectonic and non-tectonic deformation signals, residual atmospheric delay signals, measurement noise, etc. In geophysical studies, it is very important to separate various geophysical signals from the GNSS time series to truthfully reflect the effect of mass loadings on crustal deformation. Based on the independence of mass loadings, we combine the Ensemble Empirical Mode Decomposition (EEMD) with the Phase Space Reconstruction-based Independent Component Analysis (PSR-ICA) method to analyze the vertical time series of GNSS reference stations. In the simulation experiment, the seasonal non-tectonic signal is simulated by the sum of the correction of atmospheric mass loading and soil moisture mass loading. The simulated seasonal non-tectonic signal can be separated into two independent signals using the PSR-ICA method, which strongly correlated with atmospheric mass loading and soil moisture mass loading, respectively. Likewise, in the analysis of the vertical time series of GNSS reference stations of Crustal Movement Observation Network of China (CMONOC), similar results have been obtained using the combined EEMD and PSR-ICA method. All these results indicate that the EEMD and PSR-ICA method can effectively separate the independent atmospheric and soil moisture mass loading signals and illustrate the significant cause of the seasonal variation of GNSS vertical time series in the mainland of China.

**Key words:** Phase space reconstruction-based independent component analysis, ensemble empirical mode decomposition, mass loading, hurst parameter, GNSS vertical coordinate time series.

### 1. Introduction

GNSS technology has widely been applied in a variety of geophysical studies, and thousands of permanent GNSS stations have been established around the world for this purpose. Analyzing the time

series of GNSS stations in the International Terrestrial Reference Frame (ITRF) provides useful information for the study of the global plate motion, crustal deformation, and earthquakes. All these studies are based on the correct interpretation of the coordinate time series as well as on reliable and accurate station coordinates and velocities. The GNSS coordinate time series mainly consists of tectonic deformation (e.g., DRAGERT *et al.* 2001; JIANG *et al.* 2014), non-tectonic deformation (e.g., VANDAM *et al.* 1994; TIAMPO *et al.* 2004), and noise (WILLIAMS *et al.* 2004). Analyzing the non-tectonic deformation signals by geometric and physical models is crucial in studying the impacts of various geophysical phenomena on GNSS reference stations. NIKOLAIDIS (2002) applied a weighted least-square algorithm to solve the geometric model according to linear trend, annual, and semi-annual variations, and other characteristics of GNSS coordinate time series. DONG *et al.* (2002) investigated the effects of atmosphere, non-tidal ocean, snow, soil moisture, and other environmental factors on GNSS station displacements, and explained the main causes of the annual and semi-annual variations of GNSS time series. However, these geometrical model and physical model cannot directly extract mass loading signals (annual and semi-annual periods) from the GNSS time series. Therefore, a method separating the seasonal non-tectonic deformation signals from the GNSS vertical time series is in really needed.

The Independent Component Analysis (ICA) method is a blind source separation method, which can separate statistically independent source signals from multi-dimensional mixed observation signals (HYVÄRINEN and OJA 2000). If the geophysical phenomena are independent; then, the independent

<sup>1</sup> School of Geosciences and Info-Physics, Central South University, Changsha, China. E-mail: wjdai@csu.edu.cn

<sup>2</sup> Center for Research in Geomatics, Laval University, Quebec City, Canada.

component signals (ICs) decomposed by the ICA method will reflect their physical phenomena. The Phase Space Reconstruction-based Independent Component Analysis (PSR-ICA) method, a single-channel ICA method, can effectively separate the independent source signals, even though they are the same frequency (DAI *et al.* 2014). Therefore, in this study, we use the PSR-ICA method to analyze the seasonal variation of GNSS vertical coordinate time series. However, the vertical time series of a GNSS station is a non-stationary signal, and the PSR-ICA algorithm can only process stationary signal; therefore, we use an adaptive time–frequency decomposition method called Ensemble Empirical Mode Decomposition (EEMD) (WU and HUANG 2009), to process non-stationary GNSS vertical coordinate time series and extract the stationary seasonal signal.

## 2. EEMD and PSR-ICA Methods

The EEMD and PSR-ICA methods are jointly used to analyze the GNSS vertical time series based

on their respective advantages. First, GNSS vertical time series is decomposed using the EEMD method, and then, the noise signal and seasonal signal are classified and reconstructed based on the Hurst parameter (RODRIGUEZ *et al.* 2009). After that, the PSR-ICA method is used to decompose the reconstructed one-dimensional seasonal signal into several ICs that are then compared with non-tectonic crustal deformations caused by mass loadings. The data processing flow chart is shown in Fig. 1.

### 2.1. EEMD Decomposition and Extraction of the Seasonal Non-Tectonic Signal

The EEMD, as a modified EMD algorithm, which can be used to decompose a nonlinear and non-stationary time series  $x(t)$  into several Intrinsic Mode Functions (IMFs) and the residual signal (WU and HUANG 2009; HUANG *et al.* 1998). Then, the IMFs with different noise contents are classified and reconstructed based on the Hurst parameter. The general equation of the EEMD algorithm is given below:

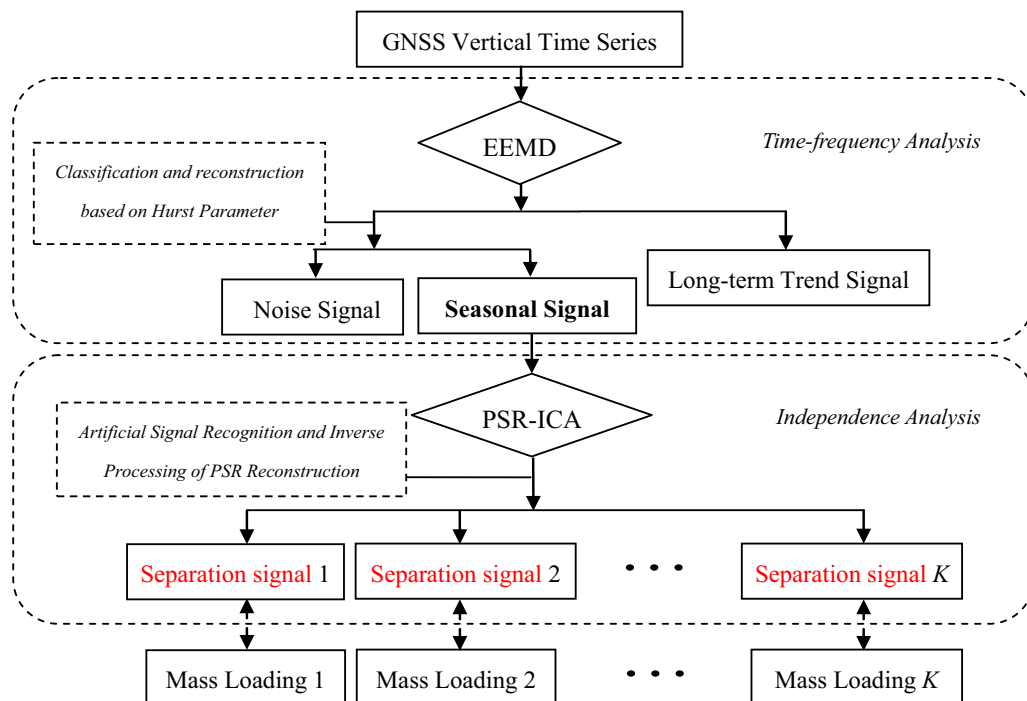


Figure 1  
Flow chart of single-channel ICA data processing for the GNSS vertical time series analysis

$$x(t) = \sum_{j=1}^D \bar{c}_j(t) + r_D(t), t = 1, 2, \dots, T \quad (1)$$

where  $\bar{c}_j(t)$  is the IMF component and  $r_D(t)$  is the residual signal.

The IMFs of the EEMD algorithm can be divided into stationary and non-stationary parts. The non-stationary IMFs can be reconstructed as a long-term trend signal (QIN *et al.* 2012), and the stationary IMFs need to be analyzed by the Hurst parameter. Hurst parameter has been used to analyze noises in many studies (MONTILLET *et al.* 2013; SCHROEDER AND WIESENFELD 1991). The relation between Hurst parameter ( $H$ ) and noise signal is that the white noise is corresponding to  $H = 0.5$ , the flick noise is corresponding to  $H = 1$  and the random walk is corresponding to  $H = 1.5$ .

The noise in the GNSS time series can be analyzed usually after removing the linear trend and seasonal variation. However, the EEMD method can decompose the noise, without removing the linear trend and seasonal variation, into a series of IMFs ordered by frequency, and these IMFs can be classified using the Hurst parameter. For example, MONTILLET *et al.* (2013) used the EMD method and the Hurst parameter to extract the white noise ( $H \leq 0.6$ ) of the GNSS vertical time series. Furthermore, several studies suggest that the best noise model of most GNSS vertical time series is the white plus flicker noise model (WN + FN) (LI *et al.* 2012; ZHANG *et al.* 1997; MAO *et al.* 1999; AMIRI-SIMKOOEI *et al.* 2007). Therefore, we define the IMFs whose  $H$  is within  $[0.6, 1.1)$  as colored noise, which can be best characterized by the WN + FN model.

The procedure of the time–frequency analysis can be described as follows.

1. Decompose time series  $x(t)$  into IMFs and residual signal.

2. Extract the non-stationary IMFs and the residual signal, and reconstruct them to long-term trend signal.
3. Estimate the Hurst parameter of each stationary IMFs. Sum over the IMFs whose  $H$  are within  $[0, 1.1]$  as noise signal, and sum over the remaining IMFs as one-dimensional seasonal signal  $x'(t)$ .

However, the EEMD method cannot decompose components in the same frequency; therefore, the one-dimensional seasonal signal should be analyzed by the single-channel ICA method.

### 2.2. Seasonal Non-Tectonic Signal Analysis by PSR-ICA Algorithm

PSR-ICA algorithm is a one-dimensional stationary signal processing method (DAI *et al.* 2014, PACKARD *et al.* 1980; TAKENS 1981), which does not rely on the time–frequency feature of the components. Therefore, it can separate ICs from the one-dimensional seasonal signals to reflect the effect of the seasonal mass loadings. The procedure of the PSR-ICA algorithm is shown in Fig. 2.

In this flow chart,  $x'$  is the one-dimensional seasonal signal;  $X$  is the reconstruction phase space;  $Y = WX$  is to obtain the ICs from the reconstruction phase space;  $X^K$  is the  $K$ th independent subspace;  $x^K$  is the reconstructed one-dimensional seasonal signal.

#### 2.2.1 Channel Extension

Phase Space Reconstruction (PSR) is a method of obtaining nonlinear dynamics features through delaying and embedding a one-dimensional signal into a high-dimensional phase space to reflect the characteristics of the signals (KENNEL *et al.* 1992). The multi-dimensional phase space contains all signals of physical sources, affecting the seasonal non-tectonic deformation of GNSS stations.

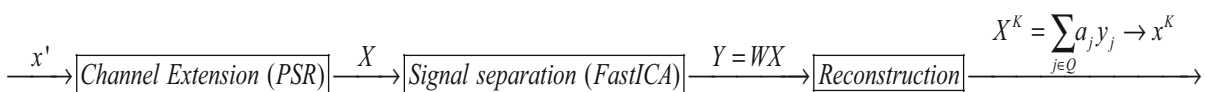


Figure 2  
Flow chart of PSR-ICA processing for the seasonal signal analysis

$$X_i = \{x'_i, x'_i(1 + \tau), \dots, x'_i(1 + (m - 1)\tau)\},$$

$$i = 1, 2, \dots, M \quad (2)$$

where  $M = T - (m - 1)\tau$ ,  $m$  is the embedding dimension,  $\tau$  is the delay time.  $m$ , and  $\tau$  are the main parameters of the PSR algorithm, whose optimal solution can be obtained using the False Nearest Neighbors method and the Mutual Information method, respectively (DAI *et al.* 2014; KENNEL *et al.* 1992; FRASER and SWINNEY 1986).

### 2.2.2 Independent Component Signal Separation

Assume a set of independent source signals  $S(t')$ :  $S(t') = [s_1(t'), s_2(t'), \dots, s_n(t')]^T$  and their corresponding observation signals  $X(t')$ :  $X(t') = [x_1(t'), x_2(t'), \dots, x_m(t')]^T$ , the relationship between  $X(t')$  and  $S(t')$  can be described as follows (HYVÄRINEN and OJA 2000):

$$X(t') = AS(t'), t' = 1, 2, \dots, M \quad (3)$$

where  $A$  is  $m \times n$ -order unknown linear mixed matrix ( $n \leq m$ ).

ICA algorithm is to separate the ICs by solving the mixed matrix  $W$ .

$$Y(t') = A^{-1}X(t') = WX(t') \quad (4)$$

ICs  $Y(t')$  can be used to estimate  $S(t')$  effectively. FastICA algorithm, a widely used ICA algorithm, is used to separate ICs from  $WX(t')$  in this study. FastICA algorithm uses the Negentropy, a measure standard of non-Gaussian distribution, to measure the non-Gaussian maximum of  $WX(t')$ , and it follows the fixed-point iteration theory, which makes the convergence faster and more robust (HYVÄRINEN 1999).

### 2.2.3 Independent Component Signals Reconstruction

These ICs  $Y(t')$  can reflect the implicit information of the observation signals. However, sometimes, the number of ICs are more than the seasonal mass loadings. Therefore, the ICs should be artificially classified into several clusters. Then, the ICs of the same cluster, corresponding to the same mass loading, are multiplied by their corresponding column of the mixed matrix to construct independent subspaces  $X^K$

for reconstructing the source signal  $x^K$  (CARDOSO 1998). Therefore, the original multi-dimensional phase space is equal to the sum of independent subspaces.

$$X = X^1 + X^2 + \dots + X^K \quad (5)$$

where  $X^K$  is the  $K$ th independent subspace, and it can be described as follows:

$$X^K = \sum_{j \in Q} a_j y_j \quad (6)$$

where  $Q$  is the number of ICs in a cluster, and  $a_j$  is the corresponding column of the mixed matrix to the  $y_j$ , where  $y_j$  is the  $j$ th IC. The independent subspaces  $X^K$  can be reconstructed to a one-dimensional source signal  $x^K$  based on the inversion of the PSR method,

$$x_i^K = \begin{cases} \frac{1}{A} \sum_{h=1}^A X_{j,i-(j-1)\tau}^K & 1 \leq i \leq 1 + (m - 1)\tau \\ \frac{1}{m} \sum_{h=1}^m X_{j,i-(j-1)\tau}^K & 1 + (m - 1)\tau \leq i \leq T - (m - 1)\tau \\ \frac{1}{B} \sum_{h=m+1-B}^m X_{j,i-(j-1)\tau}^K & T - (m - 1)\tau \leq i \leq T \end{cases} \quad (7)$$

where  $A = \text{ceil}(i/\tau)$ ,  $B = \text{ceil}((N - i + 1)/\tau)$ , and  $\text{ceil}(\cdot)$  denotes the rounding-up function.

## 3. GNSS Vertical Time Series Analysis

### 3.1. Analysis of Observation Data and Mass Loadings

The seasonal non-tectonic deformation of GNSS reference station mainly includes the mass loading of atmosphere, soil moisture, non-tidal ocean, snow, etc. However, in most parts of China, the non-tidal ocean mass loading and snow mass loading had a little or no impact on crustal deformation, and they can be neglected. Thus, the effect of atmosphere and soil moisture mass loading are the major factors in the analysis of the seasonal non-tectonic deformation (WANG *et al.* 2005).

To explore the single-channel ICA process and its effect on separating non-tectonic deformation, we use the daily vertical time series of GNSS reference stations collected by the CMONOC. These daily GNSS solutions are generated using the GAMIT/GLOBK software with the double-difference

ionosphere-free code and phase observations. Meanwhile, the station receiver antenna phase center, satellite antenna phase center, ocean tides, solid earth pole tides, and solid earth tides are corrected with the absolute phase center model, IGS ANTEX model, FES2004 ocean tide loading model, and IERS2003 model, respectively. The tropospheric delay and satellite coordinates are estimated with the station coordinates during the daily data processing, and then, each daily solutions are transformed into IGS08 using seven-parameter transformations. The data, consisting of 13 GNSS reference stations in the area from 90°E 15°N to 120°E 42°N (see Fig. 3), cover a time span from January 2001 to December 2013.

The vertical time series of those 13 GNSS stations with strong noise is manifested as non-stationary annual variation. To explore the data sets, we randomly choose three GNSS reference stations

(BJFS, JIXN, and LUZH) as proxies to demonstrate the process of our methods and its results in detail. Figure 4 shows the vertical displacement time series of BJFS, JIXN, and LUZH sites for a time interval of 13 years.

To illustrate the non-tectonic deformation in the selected area, we calculate the correction values of atmospheric and soil moisture mass loadings of the 13 sites, using the 6-hour sampling atmosphere surface pressure data and the daily sampling National Center for Environmental Prediction (NCEP) reanalysis II soil moisture data from 2001 to 2013. The corrections of mass loadings are calculated using the Quasi-Observation Combination Analysis software (QOCA) (available at <http://qoca.jpl.nasa.gov>). Results are shown in Fig. 5 for the three selected sites.

After removing the linear trend of GNSS vertical time series using the linear fitting method, the power

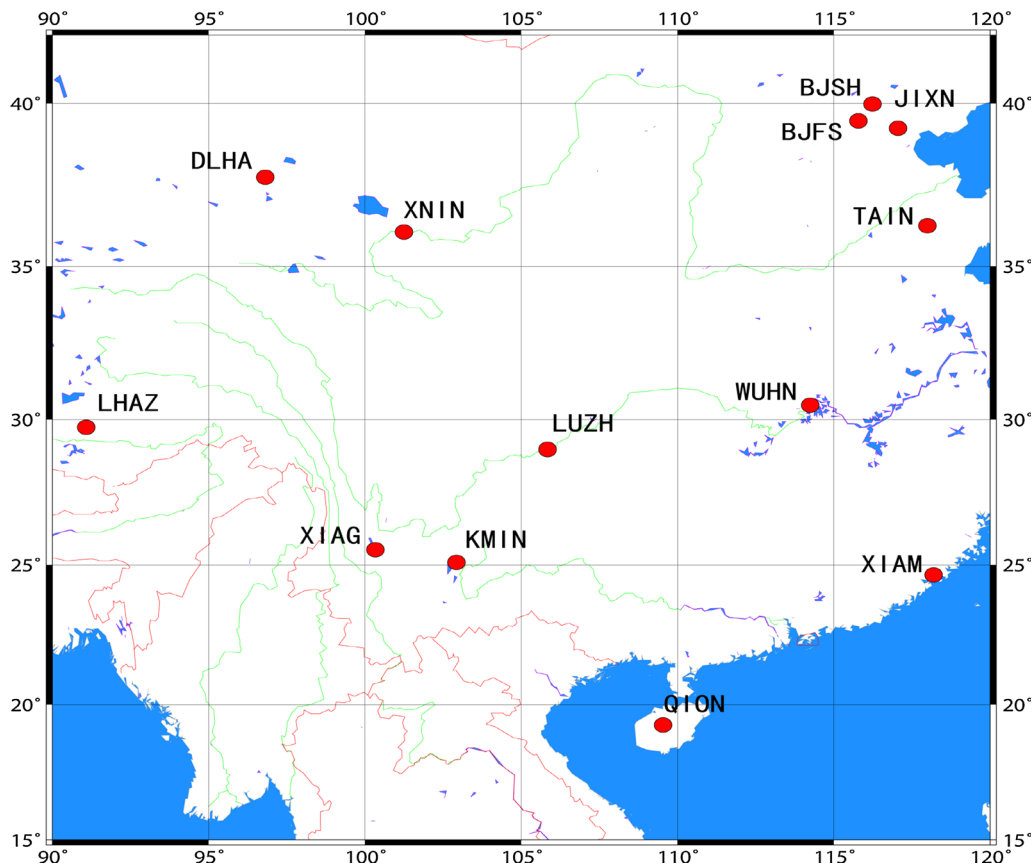


Figure 3  
Distribution of the selected CMONOC GNSS stations

spectrum is used to analyze the changes of the seasonal variation of GNSS vertical time series before and after removing the correction values of atmospheric and soil moisture mass loading, as shown in Fig. 6. After the correction, the annual variation of residual time series is significantly weakened, indicating that the correction can effectively reduce the annual variation in the GNSS vertical time series. However, the mass loading corrections cannot completely eliminate the annual variation in the GNSS reference stations. Therefore, decomposing the GNSS vertical time series into

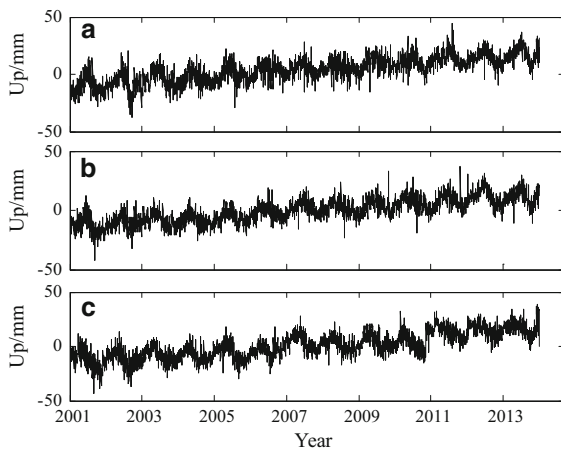


Figure 4  
Vertical time series of GNSS reference stations (a) BJFS, (b) JIXN, and (c) LUZH

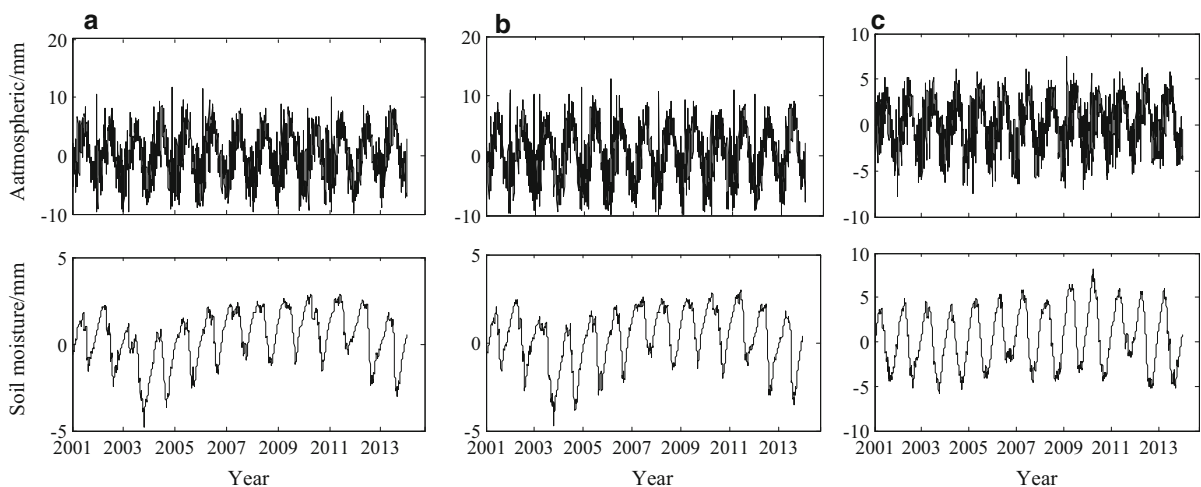


Figure 5  
Correction values of atmospheric mass loading and soil moisture mass loading (a) BJFS, (b) JIXN, and (c) LUZH

several sub-signals (relating to the main mass loadings) is an important way to illustrate the annual variation in the GNSS vertical time series.

### 3.2. EEMD Decomposition and Reconstruction

The EEMD method is used to decompose the vertical time series into IMF components and residual signal. The  $H$  values of IMFs are calculated by the Detrended Fluctuation Analysis method (GRECH and MAZUR 2013). As the calculation error can be up to 0.1, the IMFs whose  $H$  values are within  $[0, 1.1]$  are reconstructed as noise signal. The noise, the artificial reconstructed seasonal signal, and the long-term trend of BJFS, JIXN, and LUZH sites are shown in Fig. 7.

The EEMD method is also used to de-noise the sum of atmospheric mass loading and soil moisture mass loading. The comparison between the reconstructed seasonal signal and the sum of the de-noised atmospheric and soil moisture mass loadings of the 13 GNSS sites are shown in Fig. 8.

The correlation coefficients, RMS (Root Mean Square) between the seasonal signals, and the sum of the corrections of de-noised seasonal mass loadings (atmospheric mass loading and de-noised soil moisture mass loading) are calculated, and their values for the 13 GNSS stations are shown in Table 1.

The correlation coefficients of the seasonal signals and the de-noised sum of atmospheric mass loading

and soil moisture mass loading are 0.61–0.86, and  $\Delta$ RMS are 18–48 %. These results are reasonable, including the low correlation of WUHN, XNIN, KMIN, and XIAM sites (in bold), because the mass loading correction cannot completely reflect the

seasonal variation of GNSS vertical time series (see Fig. 6).

From the comparison in Fig. 8 and correlation analysis in Table 1, we can say that there is a strong correlation between the GNSS station annual variation and the two mass loadings in the selected area.

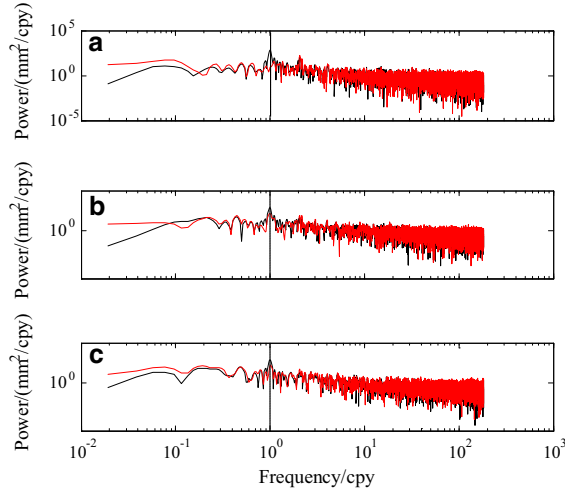


Figure 6

Power spectrum of GNSS vertical time series before (black line) and after (red line) removing the atmospheric loading and soil moisture loading **a** BJFS, **b** JIXN, and **c** LUZH

### 3.3. Simulation Experiment

We mixed the de-noised correction of the atmosphere and soil moisture mass loading (red line in Fig. 8) as the simulated non-tectonic deformation signals. First, the PSR method is applied to obtain the multi-dimensional embedding matrix, and the time delay is 8 and the embedding dimension is 2. Then, the FastICA method is used to analyze the multi-dimensional embedding matrix, and the two ICs are obtained. We rename them as Reconstructed signal A (RS-A) and Reconstructed signal B (RS-B) without artificial classification and reconstruction. The comparison of reconstructed signals and its corresponding simulated signals (de-noised atmospheric and soil moisture mass loading) are shown in Figs. 9 and 10, respectively.

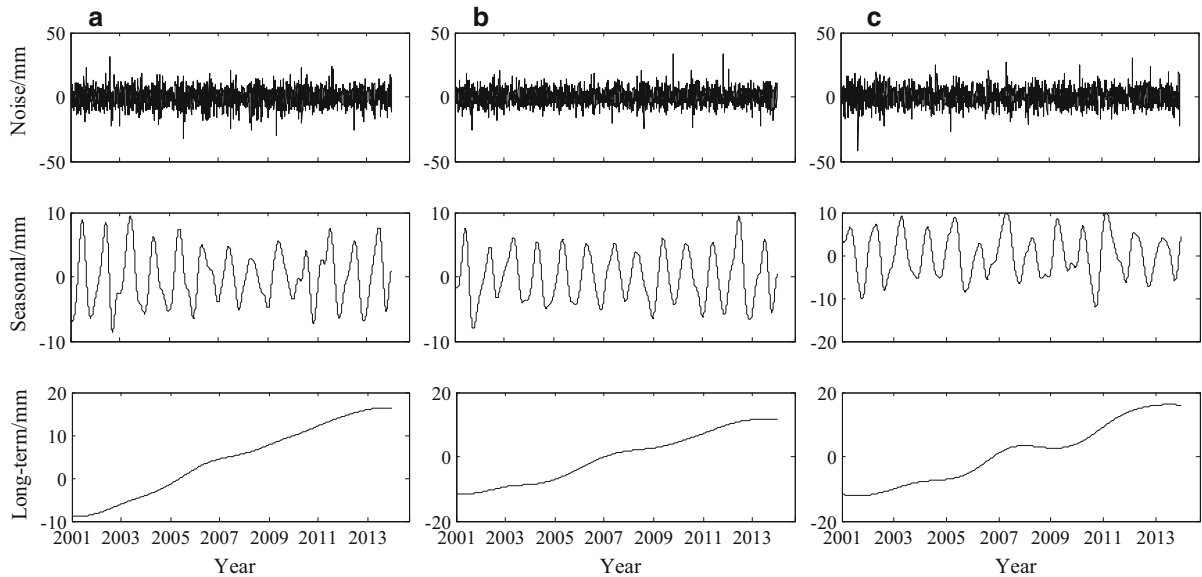


Figure 7

The reconstructed noise, seasonal signal, and long-term trend signal **a** BJFS, **b** JIXN, **c** LUZH

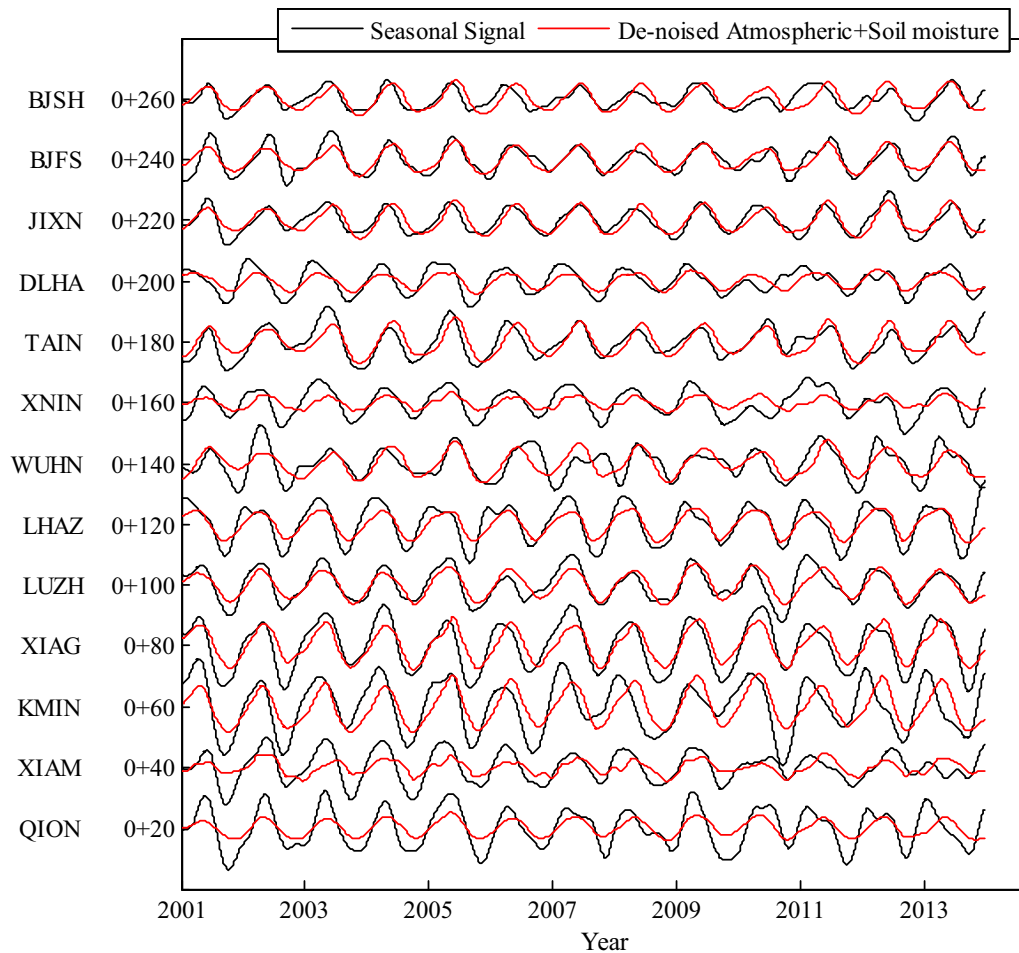


Figure 8

Comparison between the reconstructed seasonal signals decomposed by EEMD and the sum of the de-noised atmosphere and soil moisture mass loading for the 13 GNSS sites (20 mm offset per station)

The correlation coefficients and RMS between reconstructed signals and their corresponding simulation signals are calculated, respectively, and their values are shown in Table 2.

The simulation experiment shows that the signals reconstructed by the PSR-ICA method can effectively reflect the atmospheric and the soil moisture mass loading. The correlation coefficients of the RS-A and the atmospheric mass loading are 0.81–0.96, and the  $\Delta$ RMS are 11–71 %. In addition, the values of the RS-B and the soil moisture mass loading are 0.71–0.98 and 14–77 %, respectively. These facts suggest that the atmospheric and the soil moisture mass loadings can be separated by single-channel ICA.

### 3.4. GNSS Vertical Time Series Analysis

The seasonal variation of GNSS vertical time series (black line in Fig. 8) is also used to verify the effectiveness of the PSR-ICA method.

First, the time delay and the embedding dimension are calculated using the mutual information method and the FNN method, respectively. The determined time delay is 51, which is quite different from that of the simulation experiment. A possible explanation could be the difference between seasonal signal and mass loading corrections. The embedding dimension is 2 in most cases, and 3 for the KMIN site, which indicates that the ICs should be reconstructed into two main components.

Table 1

*Correlation between seasonal signals and sum of the de-noised atmospheric and soil moisture mass loading*

	Latitude N (°)	Longitude E (°)	Correlation coefficients	RMS (mm)	dRMS (mm)	$\Delta$ RMS (%)
BJSH	40.25	116.22	0.72	3.1	2.5	19
BJFS	39.61	115.89	0.86	4.2	2.2	48
JIXN	38.58	117.53	0.85	3.8	2.1	45
DLHA	37.38	97.38	0.77	4.0	2.7	33
TAIN	36.22	117.12	0.75	4.7	3.2	32
XNIN	36.60	101.77	<b>0.61</b>	4.5	3.7	<b>18</b>
WUHN	30.53	114.36	<b>0.71</b>	4.9	3.5	<b>29</b>
LHAZ	29.66	91.10	0.84	6.1	3.7	39
LUZH	28.87	105.41	0.84	5.1	2.8	45
XIAG	25.61	100.26	0.85	7.6	4.2	45
KMIN	25.03	102.80	<b>0.64</b>	8.2	6.2	<b>24</b>
XIAM	24.45	118.08	<b>0.63</b>	4.9	3.9	<b>20</b>
QION	19.03	109.85	0.79	6.3	4.6	27

dRMS RMS after mass loading correction,  $\Delta$ RMS reduction in RMS

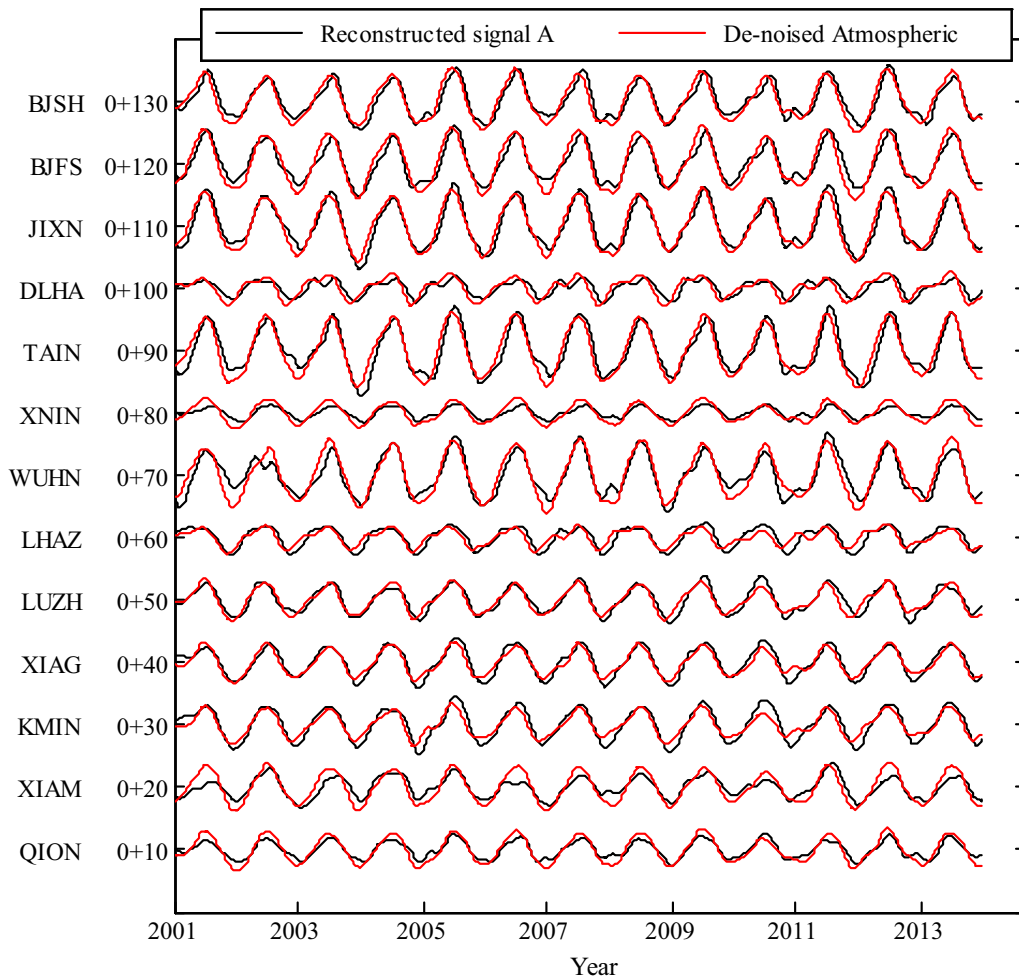


Figure 9

Comparison between the reconstructed signal A separated by PSR-ICA and the simulated signal (de-noised atmospheric mass loading) (10-mm offset per station)

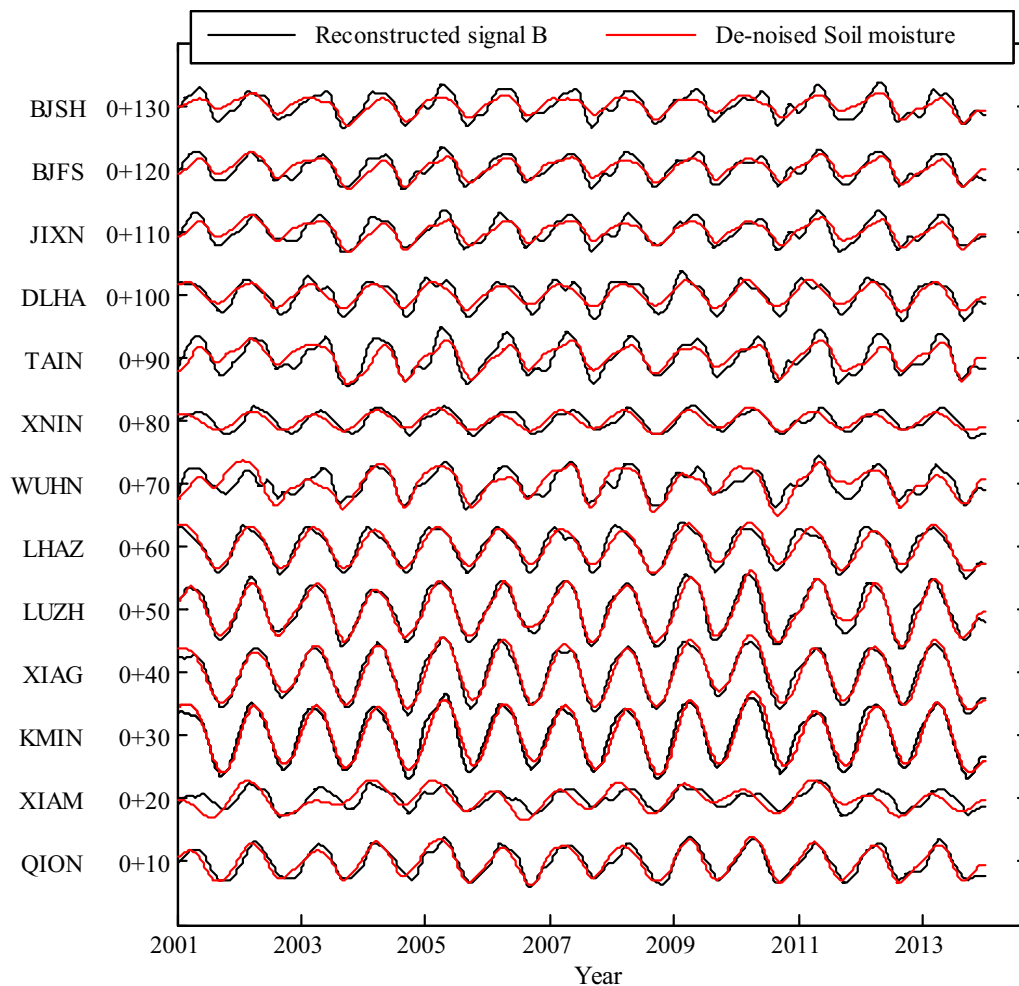


Figure 10

Comparison between the reconstructed signal B separated by PSR-ICA and the simulated signal (de-noised soil moisture mass loading) (10-mm offset per station)

Then, the FastICA method is used to separate the multi-dimensional embedding matrix. A number of ICs are obtained. Three ICs for the KMIN site are artificially reconstructed into two reconstructed signals, Reconstructed signal 1 (RS-1) and Reconstructed signal 2 (RS-2). The comparison of the two reconstructed signals for the 13 GNSS sites and their corresponding mass loadings (de-noised atmospheric and the soil moisture mass loadings) are shown in Figs. 11 and 12, respectively.

The correlation coefficients and RMS between the reconstructed signals (RS-1 and RS-2) and their corresponding mass loading signals (de-noised

atmospheric mass loading and de-noised soil moisture mass loading) are calculated, respectively, the results are shown in Table 3.

From the correlation analysis of the reconstructed signals (RS-1 and RS-2) and their corresponding mass loading signals, we can say that some physical sources affect the crustal deformation. (1) The correlation coefficients of the RS-1 and the atmospheric mass loading are between 0.50 and 0.86, and  $\Delta$ RMS are within the range of 5–47 %, which suggest that the RS-1 can be considered as a seasonal non-tectonic deformation mainly affected by the atmospheric mass loading; and (2) The correlation

Table 2

*Correlation coefficients of reconstructed signals (Reconstruction A and Reconstruction B) and their corresponding mass loading signals*

	CORR-A	RMS-A (mm)	dRMS-A (mm)	$\Delta$ RMS-A (mm)	CORR-B	RMS-B (mm)	dRMS-B (mm)	$\Delta$ RMS-B (mm)
BJSH	0.94	2.7	1.0	63	0.84	1.8	1.0	4344
BJFS	0.95	2.9	0.9	69	0.87	1.8	0.9	50
JIXN	0.96	3.4	1.0	71	0.86	1.8	1.0	44
DLHA	0.81	1.2	0.9	25	0.92	2.0	0.9	55
TAIN	0.93	3.5	1.3	63	0.85	2.4	1.3	46
XNIN	0.89	0.9	0.8	11	0.83	1.4	0.8	43
WUHN	0.92	2.9	1.2	59	0.78	2.1	1.3	38
LHAZ	0.86	1.6	0.8	50	0.95	2.5	0.8	68
LUZH	0.93	2.0	0.8	63	0.98	3.3	0.8	76
XIAG	0.94	2.2	0.8	64	0.98	3.5	0.8	77
KMIN	0.93	2.4	1.0	58	0.97	3.8	1.0	74
XIAM	0.87	1.6	1.2	25	0.71	1.4	1.2	14
QION	0.94	1.3	0.8	39	0.93	2.1	0.8	62

*Case A* RS-A and the de-noised atmospheric mass loading, *Case B* RS-B and the de-noised soil moisture mass loading, *CORR* correlation coefficient, *dRMS* RMS after mass loading correction,  *$\Delta$ RMS* reduction in RMS

coefficients of the RS-2 and the soil moisture mass loading, except for the WUHN site (in bold), are in the range of 0.50–0.83, and  $\Delta$ RMS are between 8 and 44 %, which means that the RS-2 can be considered as a seasonal non-tectonic deformation mainly affected by soil moisture mass loading. The vertical time series of WUHN station may be affected by the change of multipath effect and the instability of the station monumentation. The seasonal variation is not obvious and covered by noise and irregular trend variation in some years, which may seriously affect the seasonal signal extraction and the independent signal separation.

According to the analysis of experimental results in Sects. 3.3 and 3.4, the major mass loadings (atmospheric mass loading and the soil moisture mass loading) can be separated effectively by the single-channel ICA.

#### 4. Discussion and Conclusion

We have shown that the PSR-ICA method can separate the independent source signals from the mixed mass loading signal in the simulation experiment. However, the correlations are 4–19 % and 2–29 % lower, respectively, between the two separated signals using the PSR-ICA method and atmospheric mass loading and soil moisture mass

loading in the simulation experiment. These facts may indicate that the surface mass loadings, such as atmospheric mass loading and soil moisture mass loading, have a weak joint effect on crustal deformation in mainland China.

The PSR-ICA decomposition of the seasonal variation of GNSS vertical time series shows lower correlations with atmospheric and moisture loadings with respect to the simulation experiment. The correlations are systematically 15–20 % lower, which are mainly caused by the difference between simulated signals (simulated by the sum of the de-noised correction of the atmosphere and soil moisture mass loadings) and GNSS time series. Their correlation coefficients are 0.61–0.86, and the PSR-ICA decomposition results of these two experiments are both compared with the de-noised correction of the atmosphere and soil moisture mass loading. However, the mass loading corrections also have errors, such as for the KMIN site, there is no snow in this area during 2001 and 2013, and the snow mass loading corrections have a seasonal variation (up to 1.5 mm). The spatial resolution of mass loading data is  $2.5^\circ \times 2.5^\circ$  that mass loading corrections cannot accurately reflect the effect of mass loadings at specified points. Therefore, with the rapid increase of GNSS reference stations worldwide, the separation of mass load signals from GNSS time series is helpful to study the effect of mass loadings on the crustal

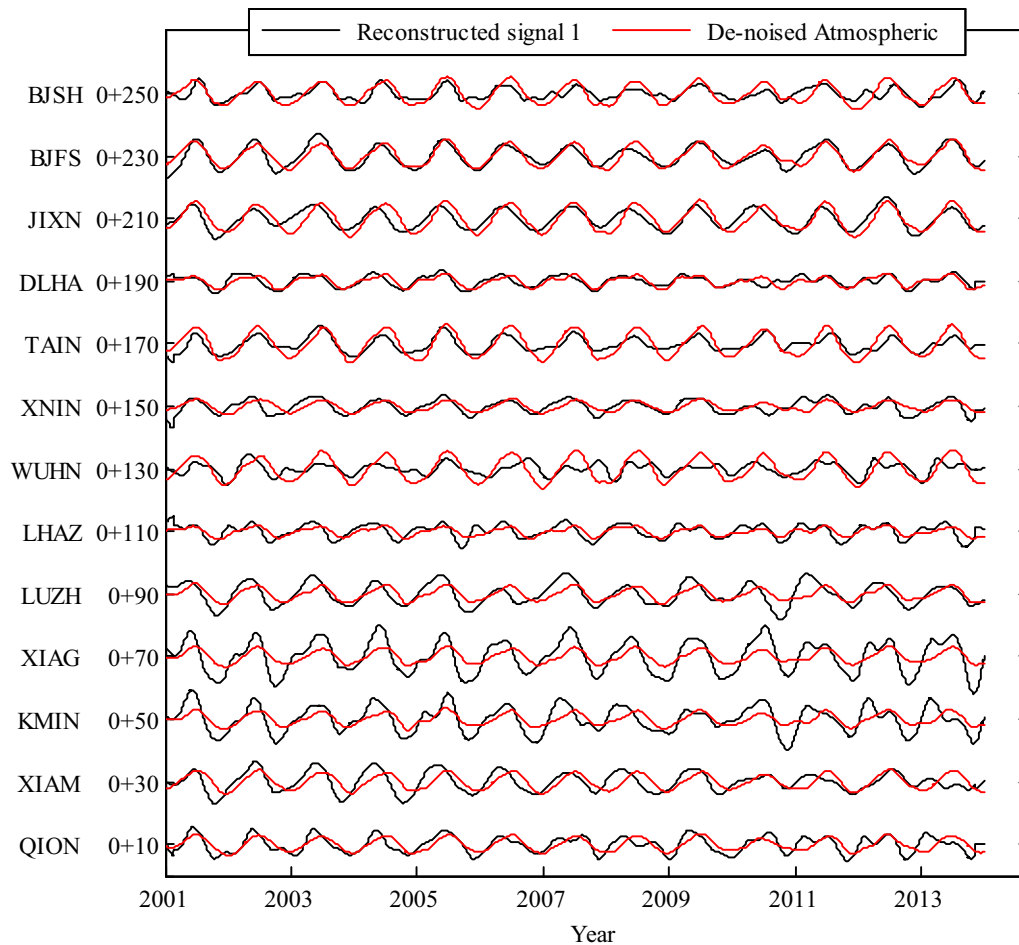


Figure 11

Comparison between the reconstructed signal 1 separated by PSR-ICA and the atmospheric mass loading (20-mm offset per station)

deformation and improve the accuracy of the correction model of mass loadings.

We use the EEMD method to decompose the GNSS vertical time series into noise signal, seasonal signal, and long-term trend signal. The PSR-ICA method is applied to analyze the seasonal signal. We successfully obtain the seasonal non-tectonic deformation signals. Through the case study of the selected GNSS reference stations, the following three conclusions can be drawn: (1) By obtaining noise signal, seasonal non-tectonic deformation signal, and long-term trend signal using the EEMD method, we found that the seasonal signal is strongly correlated with the sum of the major mass loading corrections; (2) In the

simulation experiment, the high correlation between the separated signals and mass loadings (correlation coefficients are 0.71–0.98 and  $\Delta$ RMS are 11–77 %) has proved that the PSR-ICA algorithm can accurately extract the physical source signals from the non-tectonic deformation signals; (3) The high correlation between the signals separated from seasonal signals and mass loadings (correlation coefficients are 0.50–0.86 and  $\Delta$ RMS are 5–47 %) can effectively illustrate the seasonal variation (mainly annual variation) in the vertical time series of the GNSS reference station, and the separated signals can more accurately reflect the effects of various mass loadings on the crustal deformation.

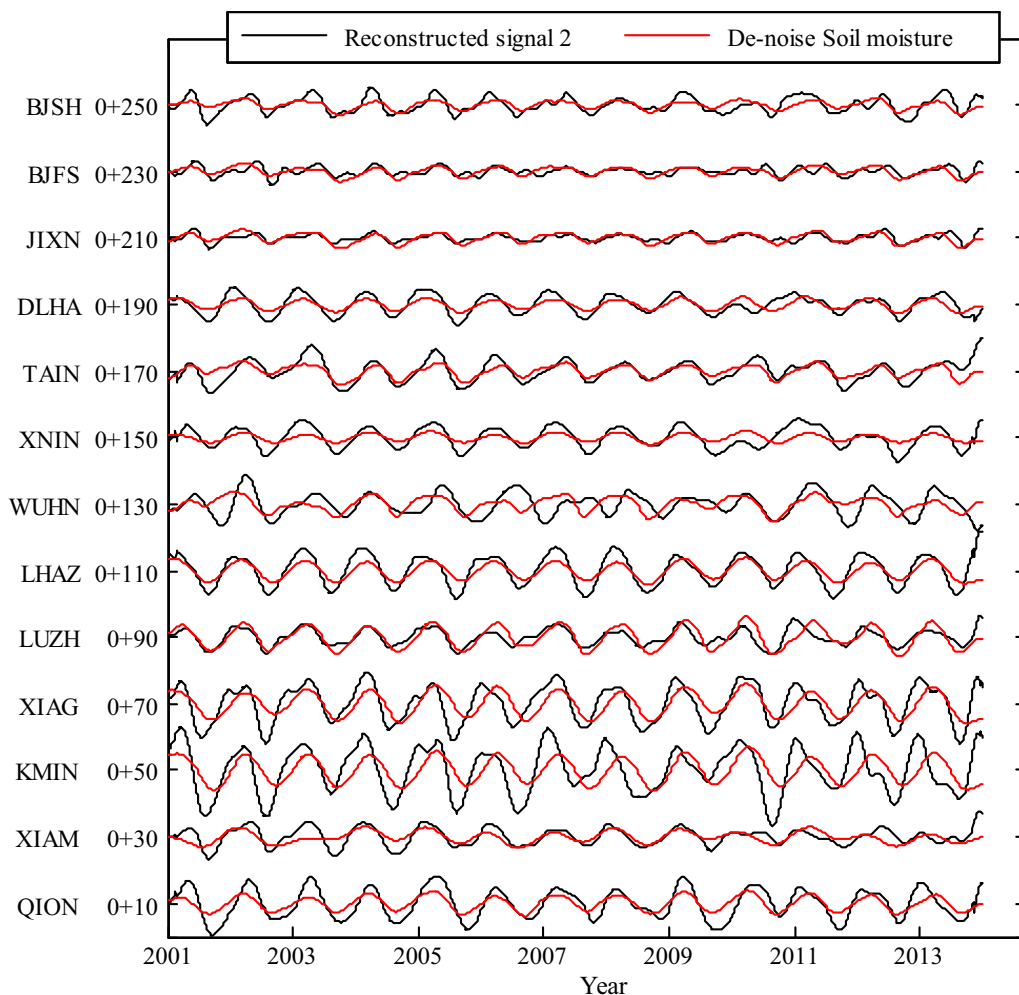


Figure 12

Comparison between the reconstructed signal 2 separated by PSR-ICA and the soil moisture mass loading (20-mm offset per station)

Table 3

Correlation between the reconstructed signals (RS-1 and RS-2) and its corresponding mass loading signals

	CORR	RMS-1 (mm)	dRMS-1 (mm)	$\Delta$ RMS-1 (%)	CORR	RMS-2 (mm)	dRMS-2 (mm)	$\Delta$ RMS-2 (%)
BJSH	0.75	1.9	1.8	5	0.71	2.4	1.8	25
BJFS	0.86	3.2	1.7	47	0.57	1.3	1.2	8
JIXN	0.79	3.0	2.0	33	0.72	1.1	0.9	18
DLHA	0.76	1.7	1.1	35	0.81	2.8	1.9	32
TAIN	0.80	2.3	2.0	13	0.75	3.2	2.2	31
XNIN	0.57	2.1	1.7	19	0.75	3.1	2.3	26
WUHN	0.61	3.5	3.2	9	<b>0.35</b>	1.9	2.9	<b>-53</b>
LHAZ	0.64	2.2	1.7	23	0.85	4.5	2.5	44
LUZH	0.62	3.4	2.7	21	0.76	2.4	2.0	17
XIAG	0.73	5.1	4.0	22	0.63	5.5	4.3	22
KMIN	0.63	4.1	3.4	17	0.50	7.0	6.3	10
XIAM	0.50	3.0	2.8	7	0.72	2.6	1.8	31
QION	0.63	2.6	2.1	19	0.83	4.4	2.9	34

Case 1 RS-1 and de-noised atmospheric mass loading, Case 2 RS-2 and de-noised soil moisture mass loading, CORR correlation coefficient, dRMS RMS after mass loading correction,  $\Delta$ RMS reduction in RMS

### Acknowledgments

We thank the Jet Propulsion Laboratory for providing the QOCA software, and Crustal Movement Observation Network of China for providing the GNSS time series. This work was supported by the State Key Development Program of Basic Research of China (Grant No. 2013CB733303) and the National Natural Science Foundation of China (Grant No. 41074004).

### REFERENCES

- AMIRI-SIMKOEI, A. R., TIBERIUS, C. C. J. M., and TEUNISSEN, S. P. (2007). Assessment of noise in GPS coordinate time series: methodology and results. *Journal of Geophysical Research: Solid Earth* (1978–2012), *112*(B7).
- CARDOSO, J. (1998). Multidimensional independent component analysis. In *Acoustics, Speech and Signal Processing. Proceedings of the 1998 IEEE International Conference*, 4, 1941–1944.
- DAI, W., HUANG, D., and LIU, B. (2014). A phase space reconstruction based single channel ICA algorithm and its application in dam deformation analysis. *Survey Review*, *47*(345), 387–396.
- DONG, D., FANG, P., BOCK, Y., CHENG, M. K., and MIYAZAKI, S. (2002). Anatomy of apparent seasonal variations from GPS-derived site position time series. *Journal of Geophysical Research: Solid Earth* (1978–2012), *107*(B4), ETG-9.
- DRAGERT, H., WANG, K., and JAMES, T. S. (2001). A silent slip event on the deeper Cascadia subduction interface. *Science*, *292*(5521), 1525–1528.
- FRASER, A. M., and SWINNEY, H. L. (1986). Independent coordinates for strange attractors from mutual information. *Physical Review A*, *33*(2), 1134.
- GRECH, D., and MAZUR, Z. (2013). On the scaling ranges of detrended fluctuation analysis for long-term memory correlated short series of data. *Physica A: Statistical Mechanics and its Applications*, *392*(10), 2384–2397.
- HUANG, N. E., SHEN, Z., LONG, S. R., WU, M. C., SHIH, H. H. *et al.* (1998). The empirical mode decomposition and the Hilbert spectrum for nonlinear and non-stationary time series analysis. In *Proceedings of the Royal Society of London A: Mathematical, Physical and Engineering Sciences* (Vol. 454, 1971, 903–995).
- HYVÄRINEN, A., and OJA, E. (2000). Independent component analysis: algorithms and applications. *Neural networks*, *13*(4), 411–430.
- HYVÄRINEN, A. (1999). Fast and robust fixed-point algorithms for independent component analysis. *Neural Networks, IEEE Transactions on*, *10*(3), 626–634.
- JIANG, Z., WANG, M., WANG, Y., WU, Y., CHE, S. *et al.* (2014). GPS constrained coseismic source and slip distribution of the 2013 mw6.6 Lushan, China, earthquake and its tectonic implications. *Geophysical Research Letters*, *41*(2), 407–413.
- KENNEL, M. B., BROWN, R., and ABARBANEL, H. D. (1992). Determining embedding dimension for phase-space reconstruction using a geometrical construction. *Physical Review A*, *45*(6), 3403.
- LI ZI, JIANG, W. P., LIU, H. F., and QU, X. C. (2012). Noise model establishment and analysis of IGS reference station coordinate time series inside China. *Acta Geodaetica et Cartographica Sinica*, *41*(4), 496G503.
- MAO, A., HARRISON, C. G., and DIXON, T. H. (1999). Noise in GPS coordinate time series. *Journal of Geophysical Research: Solid Earth* (1978–2012), *104*(B2), 2797–2816.
- MONTILLET, J. P., TREGONING, P., MCCLUSKY, S., and YU, K. (2013). Extracting white noise statistics in GPS coordinate time series. *IEEE Geoscience and Remote Sensing Letters*, *10*(3), 563–567.
- NIKOLAIDIS, R. (2002). Observation of geodetic and seismic deformation with the Global Positioning System. Ph.D. Thesis, University of California, San Diego.
- PACKARD, N. H., CRUTCHFIELD, J. P., FARMER, J. D., and SHAW, R. S. (1980). Geometry from a time series. *Physical Review Letters*, *45*(9), 712.
- QIN, Z., ZOU, X., and WENG, F. (2012). Comparison between linear and nonlinear trends in NOAA-15 AMSU-A brightness temperatures during 1998–2010. *Climate Dynamics*, *39*(7–8), 1763–1779.
- RODRIGUEZ, E., ECHEVERRIA, J. C., and ALVAREZ-RAMIREZ, J. (2009).  $1/f^2$  fractal noise generation from Grünwald-Letnikov formula. *Chaos, Solitons & Fractals*, *39*(2), 882–888.
- SCHROEDER, M., WIESENFELD, K. (1991). Fractals, chaos, power laws: minutes from an infinite paradise. *Physics Today*, *44*(11), 91–91.
- TAKENS, F. (1981). Detecting strange attractors in turbulence. *Dynamical Systems and Turbulence*, Warwick 1980. Springer, Berlin, Heidelberg, 366–381.
- TIAMPO, K. F., RUNDLE, J. B., KLEIN, W., BEN-ZION, Y., and MCGINNIS, S. (2004). Using eigenpattern analysis to constrain seasonal signals in Southern California. *Pure and Applied Geophysics*, *161*(9–10), 1991–2003.
- VANDAM, T. M., BLEWITT, G., and HEFLIN, M. B. (1994). Atmospheric pressure loading effects on Global Positioning System coordinate determinations. *Journal of Geophysical Research: Solid Earth* (1978–2012), *99*(B12), 23939–23950.
- WANG, M., SHEN, Z. K., and DONG, D. N. (2005). Effects of non-tectonic crustal deformation on continuous GPS position time series and correction to them. *Diqiu Wuli Xuebao* (Chinese Journal of Geophysics), *48*(5), 1045–1052.
- WILLIAMS, S. D., BOCK, Y., FANG, P., JAMASON, P., NIKOLAIDIS, R. M., *et al.* (2004). Error analysis of continuous GPS position time series. *Journal of Geophysical Research: Solid Earth* (1978–2012), *109*(B3).
- WU, Z., and HUANG, N. E. (2009). Ensemble empirical mode decomposition: a noise-assisted data analysis method. *Advances in Adaptive Data Analysis*, *1*(01), 1–41.
- ZHANG, J., BOCK, Y., JOHNSON, H., FANG, P., WILLIAMS, S. *et al.* (1997). Southern California permanent GPS geodetic array: Error analysis of daily position estimates and site velocities. *Journal of Geophysical Research: Solid Earth* (1978–2012), *102*(B8), 18035–18055.